EUROPEAN ORGANIZATION FOR NUCLEAR RESEARCH

DIRAC Note 2015-05
December 16, 2015

The estimation of production rates of π^+K^-, π^-K^+ and $\pi^+\pi^-$ atoms in proton-nucleus interactions at 450 GeV/c

O.Gorchakov, L.Nemenov

GENEVA
2015

Abstract

Short-lived ($\tau \sim 3 \times 10^{-15} s$) π^+K^-, $K^+\pi^-$ and $\pi^+\pi^-$ atoms as well as long-lived ($\tau \geq 1 \times 10^{-11}$ s) $\pi^+\pi^-$ atoms produced in proton-nucleus interactions at 24 GeV/c are observed and studied in the DIRAC experiment at the CERN PS. The purpose of this paper is to show that the yields of the short-lived π^+K^-, $K^+\pi^-$ and $\pi^+\pi^-$ atoms in proton-nucleus interactions at 450 GeV/c and $\theta_{lab} = 4^\circ$ are estimated to be, respectively, 17, 38 and 16 times higher per time unit. This may allow significantly improving the precision of their lifetime measurement and $\pi\pi$ and πK scattering length combinations $|a_0 - a_2|$ and $|a_{1/2} - a_{3/2}|$. The yields of the long-lived π^+K^-, $K^+\pi^-$ and $\pi^+\pi^-$ atoms at 450 GeV/c are estimated to be 370, 1600 and 750 times higher than at 24 GeV/c. This may allow the resonance method to be used for measuring the Lamb shift in the $\pi\pi$ atom and a new $\pi\pi$ scattering length combination $2a_0 + a_2$ to be obtained.

1 Introduction

The lifetime measurement of atoms consisting of K^+ and π^- ($A_{K\pi}$), K^- and π^+ ($A_{\pi K}$) and π^+ and π^- ($A_{2\pi}$) allows model-independent measurement of the $\pi\pi$ and $K\pi$ scattering lengths [1, 2, 3, 4, 5]. Experimental investigations of the $A_{K\pi}$ and $A_{2\pi}$ atoms were performed in the DIRAC experiment at the CERN PS at the proton beam momentum of 24 GeV/c [5, 6, 7, 8, 9].

The lifetime of short-lived $A_{2\pi}$ ($\tau_{th} = 2.9 \times 10^{-15} s$) is related to the $\pi\pi$ s-wave scattering length combination $|a_0 - a_2|$, where 0 and 2 are the isospin values. In the DIRAC experiment the τ was measured [6, 7] with a precision of about 9% which gives 4.3% for the $|a_0 - a_2|$ combination accuracy (statistical error 3.1%), far from the theoretical uncertainty of 1.5% [3] which can be improved using the latest results of lattice calculations.

The lifetime of short-lived $A_{\pi^+K^-}$ and $A_{K^+\pi^-}$ ($\tau_{th} = 3.5 \times 10^{-15} s$) is related to the πK S-wave scattering length combination $|a_{1/2} - a_{3/2}|$, where 1/2 and 3/2 are the isospin values. The limited number of the produced and detected short-lived $K\pi$ atoms allowed to estimate their lifetime and the $K\pi$ scattering length combination $|a_{1/2} - a_{3/2}|$ with the errors of 100% and 60% respectively [8]. The theoretical prediction of the $K\pi$ atom lifetimes and $K\pi$ scattering lengths are obtained with the 10% and 5% errors respectively [10, 11, 12, 13].

The investigation of long-lived $A_{2\pi}$ allows the Lamb shift to be measured in this atom [14, 15, 16] and another combination of the $\pi\pi$ scattering lengths $2a_0 + a_2$ to be extracted. If the resonance method can be used, this combination will be obtained with a precision an order of magnitude higher than in other methods [17, 18]. At the present time 436±61

$\pi^+\pi^-$ pairs generated in the breakup of long-lived $A_{2\pi}$ in the Pt foil have been observed in the DIRAC experiment [9].

All the dimesoatoms in DIRAC were investigated using a two-arm vacuum magnetic spectrometer with detectors placed in front of and behind the spectrometer magnet [19]. The particles generated in the target by the primary proton beam moved in the solid angle of $1.2 \times 10^{-3} sr$ and crossed all the detectors in front of the magnet. Positive and negative particles that crossed the detectors behind the magnet had the momentum in the interval of 1.2-7 GeV/c. The flux of the secondary particles through the detectors restricts the primary proton beam intensity and atoms production rate per time unit. In the short-lived and long-lived dimesoatom studies the primary proton beam intensity was 10^{11}protons/spill and 3×10^{11}protons/spill (with the spill time of 0.45 s) respectively. The short-lived atoms were generated in the Ni and Pt targets. Moving in the target, they interacted electromagnetically with the target atoms, and part of them were broken up producing $\pi^+\pi^-$ ($K\pi$) pairs with a small relative momentum Q in the pair c.m.s. (atomic pair). The free $\pi^+\pi^-$ ($K\pi$) pairs were also produced in the same target. The corresponding background of these free pairs at small Q was larger than the dimesoatom signal by more than an order of magnitude. This background gives the largest contribution to the error of the atomic pair number.

Observation of the long-lived $A_{2\pi}$ atoms in the DIRAC experiment is based on the following scheme. First, short-lived ns states are produced in the Be target. Moving in the target and electromagnetically interacting with Be atom some part of them leave the target in excited long-lived states with different quantum numbers. These atoms in the momentum interval of 2.5-10.5 GeV/c have the decay length from a few centimeters up to 3.4 meters in the l.s. [14]. The Pt foil with thickness of 2.1 μ was installed at a distance of 96 mm downstream of the Be target More than 90% of the long-lived atoms are broken up into $\pi^+\pi^-$ atomic pairs in this foil. The week magnetic field between the Be target and the Pt foil was applied to enlarge the vertical component Q_Y of the relative momentum Q in the c.m.s. of the $\pi^+\pi^-$ pairs generated in the Be target. The increased Q_Y allows suppressing the background of the $\pi\pi$ pairs produced in the Be target. However, this magnetic field practically did not reduce the flux of the charged particles into the setup aperture.

It is obvious that for the investigation of the $K\pi$ atoms and improvement of the $\pi\pi$ atom Lamb shift and lifetime measurement accuracy, the detected number of atoms must be increased by more than an order of magnitude. A significant increase in the dimesoatom yields when the incident proton momentum increased from 24 GeV/c to 450 GeV/c (on the SPS CERN) was shown in [20, 21, 22]. The yields and spectra of $A_{2\pi}$, $A_{\pi^+K^-}$ and $A_{\pi^-K^+}$ generated in pNi interactions at 24 and 450 GeV/c were calculated in [22] a bit more precisely than in [20, 21]. Because the yields of $A_{\pi^+K^-}$, $A_{\pi^-K^+}$ and $A_{2\pi}$ at 24 GeV/c and $\theta_{lab} = 5.7^\circ$ are measured now, the ratio of these yields at 450 GeV/c, $\theta_{lab} = 0 - 5.7^\circ$ and at 24 GeV/c were calculated. It allows determining the optimal value of θ_{lab} at 450 GeV/c and expected statistics of $A_{2\pi}$ and $A_{\pi K}$.

The yields of $K^\pm$- and $\pi^\pm$-mesons were obtained in [22] by the computer simulation programs FRITIOF 6.0 and JETSET 7.3 [23].

In the present work the calculations are performed using the FTF generator [24], which is a developed version of FTITIOF generator for GEANT4 [25]. There are no experimental data on inclusive $\pi^\pm$ and $K^\pm$ production in pNi-interactions at 24 GeV/c. Therefore, to estimate the FTF precision in describing these data we compare the FTF predictions

with the experimental data on inclusive $\pi^{\pm}$ and $K^{\pm}$ production in pC interactions at 31 GeV/c [27] (in the same angle intervals as in the DIRAC experiment). The experimental data from pC and pCu interactions at 100 GeV/c [29] are also compared with the generator predictions to make the conclusion about FTF ability to describe inclusive cross sections for both nuclei. The FTF accuracy at 450 GeV/c was checked only in the laboratory angle interval 0-1.7° where there are experimental data [28]. The absolute and relative dimesoatom yields at 450 GeV/c as a function of θ_{lab} and atom momentum are calculated. It allows obtaining the expected number of detected short-lived and long-lived dimesoatoms and possible statistical errors.

2 Basic relations

The atom production probability is proportional to the double inclusive cross section for generation of two constituent particles of this atom with small relative momenta. Calculating the atom production cross section, one should exclude the contribution to the double cross section from those constituents that arise from the decays of long-lived particles and cannot form the atom. When one or both particles in the pair come from these decays the typical range between them is much larger than the Bohr radius of the atom (249 fm for $A_{\pi K}$ and 387 fm for $A_{2\pi}$) and the atom production probability is negligible. The main long-lived sources of pions are η and η'. In the case of pions and kaons, the main contribution comes from the short-lived sources.

The laboratory differential inclusive cross section for the atom production can be written in the form [14]

$$\frac{d\sigma_n^A}{d\vec{p}_A} = (2\pi)^3 \, \frac{E_A}{M_A} \, |\Psi_n(0)|^2 \; \left. \frac{d^2\sigma_s}{d\vec{p}_1 \, d\vec{p}_2} \right|_{\vec{p}_1 = \frac{m_1}{m_2}\vec{p}_2 = \frac{m_1}{M_A}\vec{p}_A} , \qquad (1)$$

where M_A is the atom mass, $\vec{p}_A$ and E_A are the momentum and energy of the atom in the lab system, respectively, $|\Psi_n(0)|^2 = p_B^3/\pi n^3$ is the atomic wave function (without regard for the strong interactions between the particles forming the atom, i.e., it is the pure Coulomb wave function) squared at the origin with the principal quantum number n and the orbital momentum $l = 0$, p_B is the Bohr momentum of the particles in the atom, $d^2\sigma_s^0/d\vec{p}_1 d\vec{p}_2$ is the double inclusive production cross section for the pairs from the short-lived sources (hadronization processes, ρ, ω, Δ, K^*, Σ^*, etc.) without regard for the $\pi^+\pi^-$ ($K^+\pi^-$, $K^-\pi^+$) Coulomb interaction in the final state, and $\vec{p}_1$ and $\vec{p}_2$ are the momenta of the particles forming the atom in the lab system. The momenta obey the relation $\vec{p}_1 = \frac{m_1}{m_2}\vec{p}_2 = \frac{m_1}{M_A}\vec{p}_A$ (m_1 and m_2 are the masses of the particles). The atoms are produced with the orbital momentum $l = 0$, because $|\Psi_{n,l}(0)|^2 = 0$ when $l \neq 0$. The atoms are distributed over n as n^{-3}: $W_1 = 83\%$, $W_2 = 10.4\%$, $W_3 = 3.1\%$, $W_{n\geq 4} = 3.5\%$. Note that $\Sigma_{n=1}^{\infty}|\Psi_n(0)|^2 = 1.202|\Psi_1(0)|^2$.

After substituting the expression for $|\Psi_n(0)|^2$ and summing over n, one can obtain an expression for the inclusive yield of atoms in all S-states through the inclusive yields of positive and negative hadron pairs

$$\frac{d\sigma^A}{d\vec{p}_A} = \; 1.202 \times 8 \, \pi^2 \, (\mu\alpha)^3 \, \frac{E_A}{M_A} \; \left. \frac{d^2\sigma_s}{d\vec{p}_1 \, d\vec{p}_2} \right|_{\vec{p}_1 = \frac{m_1}{m_2}\vec{p}_2 = \frac{m_1}{M_A}\vec{p}_A} , \qquad (2)$$

where μ is the reduced mass of the atom ($\mu = \frac{m_1 m_2}{m_1+m_2}$), and α is the fine structure constant.

Instead of the differential cross section, it is convenient to introduce the particle production probability per inelastic interaction (yield)

$$\frac{dN}{d\vec{p}} = \frac{d\sigma}{d\vec{p}}\,\frac{1}{\sigma_{in}}, \qquad \frac{d^2N}{d\vec{p_1}d\vec{p_2}} = \frac{d^2\sigma}{d\vec{p_1}d\vec{p_2}}\,\frac{1}{\sigma_{in}}, \tag{3}$$

where σ_{in} is the inelastic cross section of hadron production.

Then

$$\frac{dN_A}{d\vec{p}_A} = 1.202 \times 8\,\pi^2\,(\mu\alpha)^3\,\frac{E_A}{M_A}\,\left.\frac{d^2N_s}{d\vec{p_1}\,d\vec{p_2}}\right|_{\vec{p}_1=\frac{m_1}{m_2}\vec{p}_2=\frac{m_1}{M_A}\vec{p}_A}, \tag{4}$$

The double yield (without regard for the Coulomb interaction) can be presented as [30]:

$$\frac{d^2N_s}{d\vec{p_1}d\vec{p_2}} = \frac{dN_1}{d\vec{p_1}}\,\frac{dN_2}{d\vec{p_2}}\,R(\vec{p_1},\vec{p_2},s), \tag{5}$$

where $dN_1/d\vec{p_1}$ and $dN_2/d\vec{p_2}$ are the single-particle yields, R is a correlation function due to strong interaction only, and s is the c.m.s. energy squared.

The $A_{2\pi}$ yield was measured [7] at 24 GeV/c and $\theta_{lab} = 5.7°$, the yields of π^+K^- and $K^+\pi^-$ atoms at the same proton momentum and angle were obtained in [8]. Hence it is useful to present not only the absolute yields of the atoms at different conditions but also their yields relative to the known values.

3 Experimental values of pion and kaon inclusive cross sections and their description by FTF.

It is important to know how well the inclusive cross sections obtained by the FTF describe the corresponding experimental data at 24 and 450 GeV/c. The main pion momentum interval in $\pi^+\pi^-$ atomic pairs in the DIRAC experiment is 1-3 GeV/c, and for kaons from the $A_{\pi K}$ breakup it is 4-7 GeV/c. We are going to use Ni target but there is no data for pion and kaon inclusive cross sections for this material. The data [31] reveal the weak dependence of the soft pion and kaon yields on the nucleon atomic number A from Be to Cu. The weak dependence of these yields on A is also observed [29] in p-nucleus (C, Al, Cu) interactions at 100 GeV/c for the secondary particle momentum of 30 GeV/c. Therefore, the experimental soft particle yields in carbon and Be can be used to check the FTF precision, and then one may assume that the same degree of agreement of the FTF predictions with the data exists for pNi interactions.

3.1 Comparison of experimental inclusive cross sections in pC interactions at 31 GeV/c with FTF predictions.

The inclusive cross sections of π^+, π^-, K^+, and K^- in pC interactions at 31 GeV/c were measured with high precision and compared with the VENUS, EPOS and GiBUU predictions in [27]. The Figures 1 and 2 present the experimental and calculated inclusive yields of π^+, π^-, K^+, and K^- in this experiment as a function of the particle momentum in l.s. The intervals of the π^+ and π^- polar angle θ_{lab} in l.s. from 60 to 100 mrad and

from 100 to 140 mrad fully cover the θ_{lab} interval of the DIRAC setup (82-116 mrad). From Fig.1 we can see that the FTF predictions describe the inclusive cross sections in the momentum interval 1-3 GeV/c with an accuracy better than 10%.

For K^+ inclusive yields in a broad θ_{lab} interval of 20-140 mrad (Fig.2) the calculated values are 30% higher than the experimental ones.

For K^-, the calculated values in the interval 60-140 mrad are ≈15 % higher than the experimental data (Fig.2) at p_K =4 GeV/c and ≈100 % higher at p_K = 7 GeV/c.

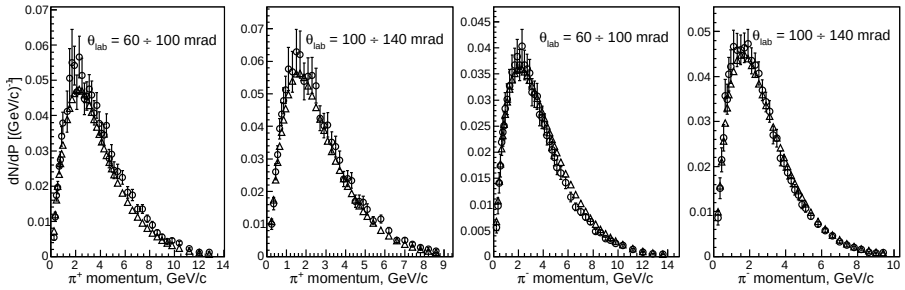

Figure 1: The yields of π^+ and π^- in pC interactions at 31 GeV/c for polar angles of 60-100 and 100-140 mrad. ○ - are the experimental data [27] and △ - are the FTF simulation data.

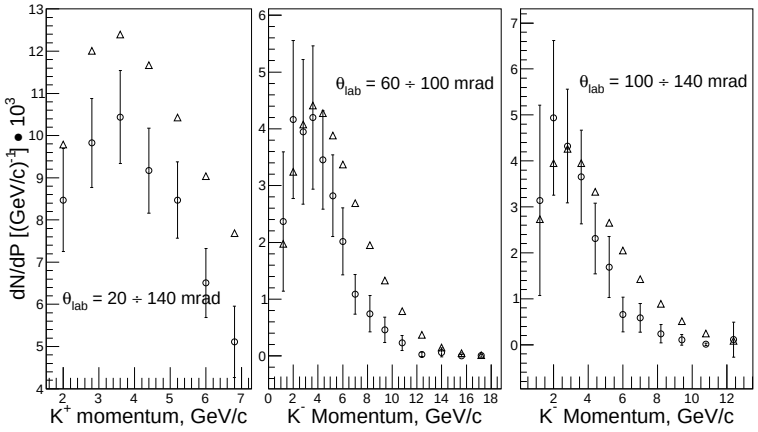

Figure 2: The yields of K^+ in pC interactions at 31 GeV/c for polar angles of 20-140 and K^- for angles 60-100 and 100-140 mrad. ○ - are the experimental data [27] and △ - are the FTF simulation data.

3.2 Comparison of experimental inclusive cross sections in p-nucleus interactions at 450 GeV/c and 100 GeV/c with FTF predictions.

The invariant inclusive cross sections of π^+, π^-, K^+ and K^- in pBe interactions at 450 GeV/c were measured in [28] and compared with FTF predictions in [26]. It was shown that the generator described well the inclusive cross sections of π^+ and π^- up to

the momentum of 70 GeV/c (Fig.3, bottom). Therefore, the generator can be used for description of $A_{2\pi}$ yields up to the momentum of 140 GeV/c.

The inclusive cross sections of K mesons are described with an accuracy of about 20% up to the momentum of 20 GeV/c and 40 GeV/c for K^+ and K^- respectively (Fig.3, bottom). It allows the yields of $A_{K\pi}$ and $A_{\pi K}$ to be calculated up to the momentum of 26 GeV/c and 51 GeV/c respectively.

The data on the dependence of the experimental inclusive yields of the π and K mesons with the momenta of 15 GeV/c and 40 GeV/c on p_t are described [26] by the FTF well (Fig.3, top).

The data on the inclusive production of π^+, π^-, K^+, and K^- in the pC and pCu interactions at 100 GeV/c [29] were compared with the FTF predictions in [26]. It was shown that the FTF did not describe the experimental data at large x for the pC interactions. The disagreement between the FTF predictions and the experimental pCu data was smaller than for the pC interactions. It can be considered as the indication that the yield of dimesoatoms at 450 GeV/c with the Ni target can be described by the FTF not worse than with the Be target.

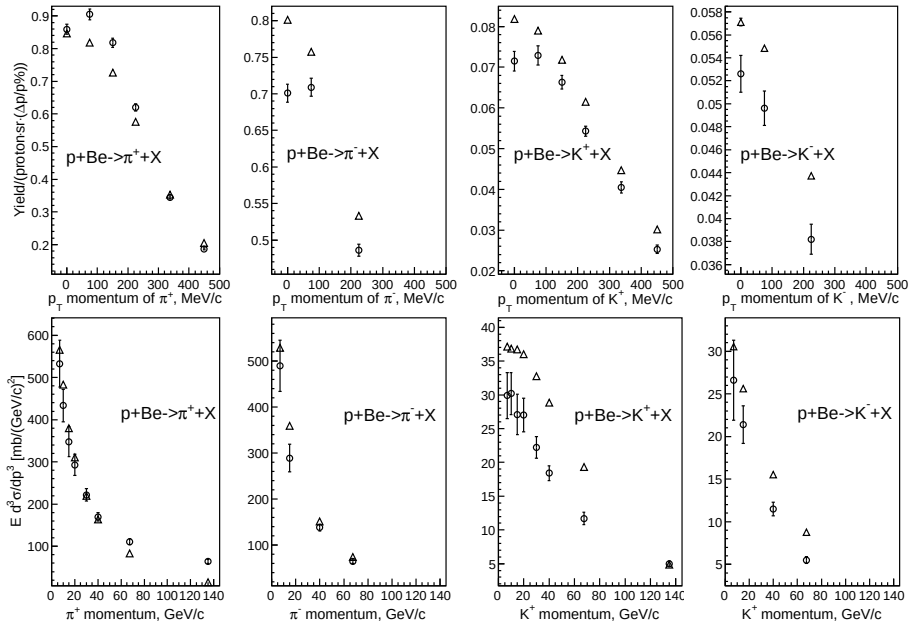

Figure 3: Top: the yields of π^+, π^-, K^+ and K^- in the pBe interactions at 450 GeV/c as a function of p_t. Bottom: the invariant inclusive cross sections of π^+, π^-, K^+ and K^- in the pBe interactions at 450 GeV/c as a function of the particle momentum in the forward direction. $\bigcirc$ - are the experimental data [27] and $\triangle$ - are the FTF simulation data.

4 Results of calculations

The selection of particles from the long-lived and short-lived sources was performed. Further, using yields from the short-lived sources only we obtained the double inclusive yields of the $\pi^+\pi^-$, $K^+\pi^-$ and $K^-\pi^+$ pairs and the dependence of corresponding atom yields on their angle and momentum in l.s.

It is important to know the ratio between the number of the dimesoatoms and the full flux of the charged particles in the same solid angle, which is seven orders of magnitude higher than the number of atoms. This flux of the charged particles restricts the intensity of the primary proton beam and consequently the number of generated atoms per time unit. Therefore, the yield of charged particles was also calculated for each angle and proton momentum.

4.1 Calculations of inclusive yields of charged particles, $\pi\pi$ and πK atoms.

In this subsection the yield is calculated in the solid angle of $10^{-3}sr$ without allowance for the setup acceptance and particle decays.

Figure 4 shows the total yields of the charged particles ($\pi^{\pm}$, $K^{\pm}$, p and $\bar{p}$) per pNi interaction event at 450 GeV/c and an emission angles $\theta_{lab} = 0°$, $2°$, $4°$ (right) and at 24 GeV/c and an emission angle $\theta_{lab} = 5.7°$ (left) as a function of their momentum.

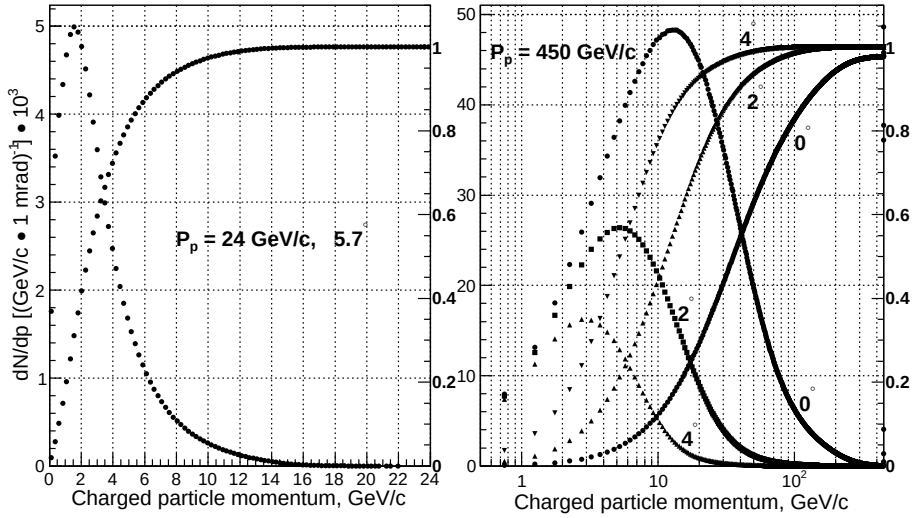

Figure 4: The total yield of the charged particles ($\pi^{\pm}$, $K^{\pm}$, p and $\bar{p}$) per pNi interaction event at 450 GeV/c and an emission angles $\theta_{lab} = 0°$, $2°$, $4°$ (right) and at 24 GeV/c and emission angle $\theta_{lab} = 5.7°$ (left) as a function of their momentum in l.s. for the solid angle of 10^{-3} sr. The integrated and normalized to 1 distributions are shown.

The yields of all the atoms into solid angle of 10^{-3} sr are shown at the top of in Fig.5. In the middle of Fig.5 the same yields of $A_{2\pi}$, $A_{\pi^+K^-}$ and $A_{K^+\pi^-}$ as a function of their momentum are presented in the intervals 2.5-10.5 GeV/c ($A_{2\pi}$) and 5-14 GeV/c ($A_{\pi K}$). The chosen intervals are the working intervals of the DIRAC setup in which identification of charged particle is really simple.

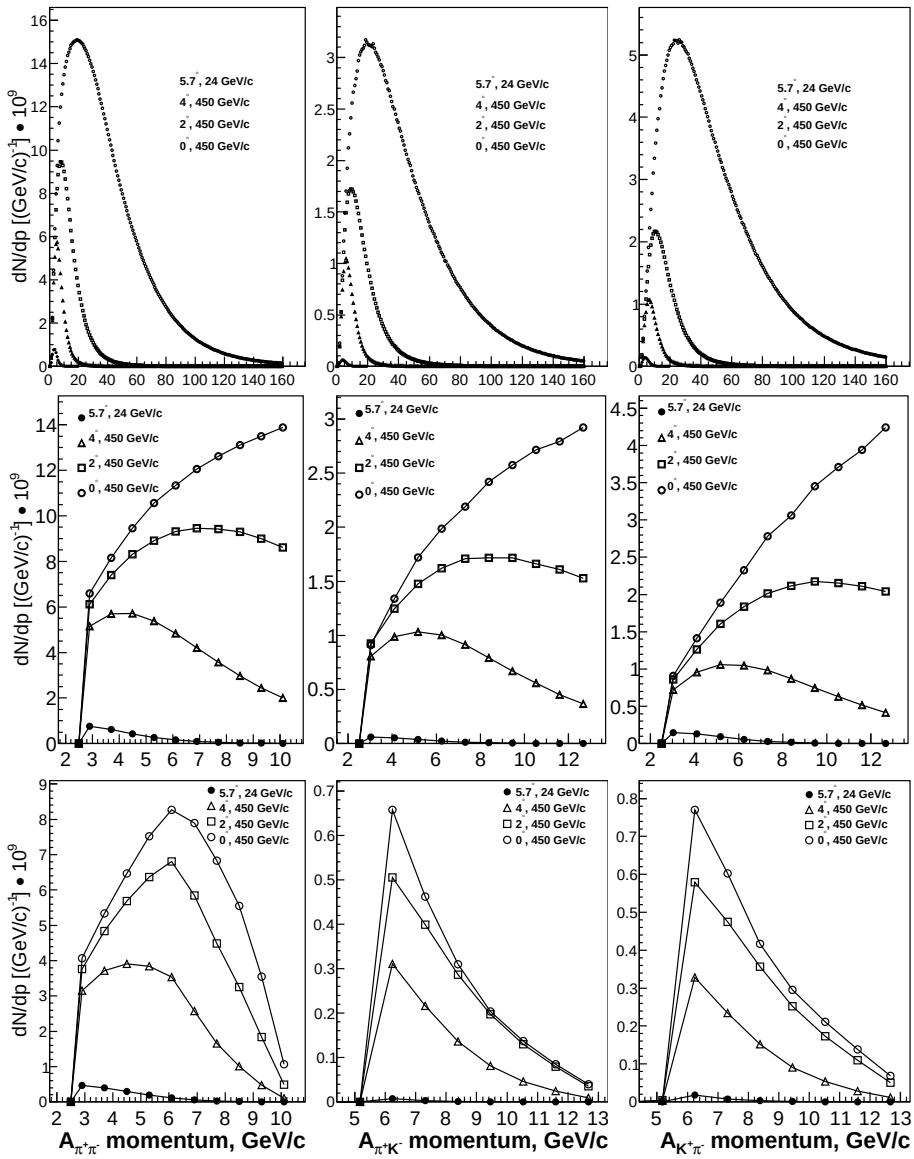

Figure 5: Yields of $A_{2\pi}$, $A_{\pi K}$ and $A_{K\pi}$ per pNi interaction event at 450 GeV/c and emission angles $\theta_{lab} = 0°$, $2°$, $4°$ and at 24 GeV/c and an emission angle $\theta_{lab} = 5.7°$ as a function of the atom momentum in l.s for the solid angle of 10^{-3} sr. Top: the DIRAC setup acceptance and decays of pions and kaons are ignored. Middle: the momentum interval of the setup is taken into account only. Bottom: the acceptance of the setup and the pion and kaon decays are taken into account.

Table 1 presents these yields integrated over p_A , where W_{ch} and W_A are the total yields of the charged particles ($\pi^{\pm}$, $K^{\pm}$, p, $\bar{p}$) and the $\pi^+\pi^-$, π^+K^-, and $K^+\pi^-$ atoms respectively into the aperture of 10^{-3} sr per pNi interaction event at 450 and 24 GeV/c. The relative yields of the charged particles and atoms at 450 and 24 GeV/c are W^N_{ch}=$W_{ch}/W_{ch}(5.7°, 24\ GeV/c)$ and W^N_A=$W_A/W_A(5.7°, 24\ GeV/c)$). The yield of $A_{2\pi}$ and $A_{\pi K}$ are practically the same as in [22] where the FRITIOF 6 code was used for calculations.

The yields of the $\pi^+\pi^-$, π^+K^- and $K^+\pi^-$ atoms at $\theta_{lab} = 4°$ and at 450 GeV/c are

Table 1: The total yields of charged particles ($\pi^{\pm}$, $K^{\pm}$, p and $\bar{p}$) W_{ch} and the $\pi^+\pi^-$, π^+K^-, and $K^+\pi^-$ atoms W_A into the aperture of 10^{-3} sr per pNi interaction event at 24 and 450 GeV/c versus the emission angle θ_{lab} in the intervals 2.5-10.5 GeV/c ($A_{2\pi}$) and 5-14 GeV/c ($A_{\pi K}$) without allowance for the decays of pions and kaons in the setup. The relative yields of the charged particles and atoms are W_{ch}^N=$W_{ch}/W_{ch}(5.7^\circ, 24\ GeV/c)$ and W_A^N=$W_A/W_A(5.7^\circ, 24\ GeV/c)$.

θ_{lab}	5.7°	4°	2°	0°
p_p	24 GeV/c	450 GeV/c	450 GeV/c	450 GeV/c
Yield of charged particles				
W_{ch}	0.022	0.14	0.50	2.9
W_{ch}^N	1	6.4	22.7	132
Yield of $\pi^+\pi^-$ atoms				
$W_A \times 10^9$	1.94	34	69	89
W_A^N	1	17.3	35.4	45.9
Yield of π^+K^- atoms				
$W_A \times 10^9$	0.217	8.1	16.3	23
W_A^N	1	37.5	75.	106.
Yield of $K^+\pi^-$ atoms				
$W_A \times 10^9$	0.52	8.5	19	30
W_A^N	1	16.4	37.6	57.4

17, 37 and 16 times higher respectively than at 24 GeV/c and $\theta_{lab} = 5.7^\circ$. These yields and the corresponding ratios at 450 GeV/c and $\theta_{lab} = 2^\circ$ are twice as high.

4.2 Calculations of inclusive yields of $\pi\pi$ and πK atoms detected by the setup

The acceptance of the DIRAC setup for πK and $\pi\pi$ atoms detection at 24 GeV/c without allowance for the particle decays is presented in Fig.6. We used the same acceptance at 450 GeV/c to obtain the yield that allows calculating the expected number of $A_{2\pi}$, $A_{\pi^+K^-}$ and $A_{K^+\pi^-}$ at 450 GeV/c using the DIRAC experimental data.

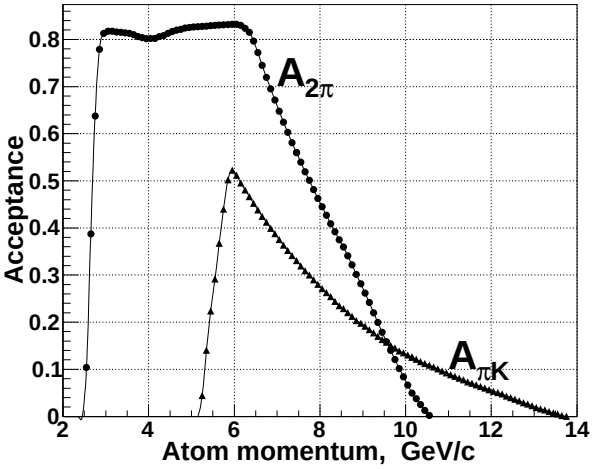

Figure 6: The acceptance of the DIRAC setup at 24 GeV/c for $A_{2\pi}$ and $A_{\pi K}$ as a function of the atom momentum. Decays of pions and kaons are not taken into account.

Table 2: The yield of the $\pi^+\pi^-$, π^+K^- and $K^+\pi^-$ atoms W_A into the aperture of 10^{-3} sr with allowance for the setup acceptance and pion and kaon decays per pNi interaction event at 24 and 450 GeV/c versus the emission angle θ_{lab}. W_A^N=$W_A/W_A(5.7°, 24\ GeV/c)$ and $(W_A/W_ch)^N$=$(W_A/W_ch)/((W_A/W_ch)(5.7°, 24\ GeV/c))$.

θ_{lab}	5.7°	4°	2°	0°
E_p	24 GeV/c	450 GeV/c	450 GeV/c	450 GeV
Yield of $\pi^+\pi^-$ atoms				
$W_A \times 10^9$	1.25	19	35	45
W_A^N	1	15	28	36
$W_A/W_{ch} \times 10^9$	57	140	70	16
$(W_A/W_{ch})^N$	1	2.4	1.2	0.27
Yield of π^+K^- atoms				
$W_A \times 10^9$	0.013	0.88	1.7	2.0
W_A^N	1	67	131	154
$W_A/W_{ch} \times 10^9$	0.59	6.3	3.4	0.69
$(W_A/W_{ch})^N$	1	10.6	5.8	1.2
Yield of $K^+\pi^-$ atoms				
$W_A \times 10^9$	0.031	0.97	2.1	2.7
W_A^N	1	31	68	87
$W_A/W_{ch} \times 10^9$	1.4	6.9	4.2	0.93
$(W_A/W_{ch})^N$	1.	4.9	3.0	0.66

The yields of $A_{\pi^+K^-}$, $A_{K^+\pi^-}$ and $A_{2\pi}$ per pNi interaction event into solid angle of 10^{-3} sr with allowance for the setup acceptance are presented in Fig.5 (bottom) as a function of the atom momentum.

These yields integrated over p_A are shown in Table 2. together with the relative yields (the yield at 24 GeV/c and 5.7° is set to 1) and the yields relative to the flux of the charged particles. The latter values are important since the DIRAC forward detectors should operate at this flux of the charged particles. Also this ratio is less sensitive to the accuracy of the meson production inclusive cross sections than the atomic absolute yield.

The yields of the $\pi^+\pi^-$, π^+K^- and $K^+\pi^-$ atoms at 450 GeV/c and $\theta_{lab} = 4°$, where charged particle momenta are small and their identification is relatively simple, are 15, 67, and 31 times higher respectively than at 24 GeV/c and $\theta_{lab} = 5.7°$. It means that it is possible to decrease the proton beam intensity to reduce of trigger events with accidental coincidences. The additional increase in the atom production is connected with the beam time during the supercycle on the PS and SPS. The DIRAC experiment on the PS had four spills with a duration of 0.45 s (full time 1.8 s) at the best conditions. On the SPS the beam time during the same supercycle is 4.6*2 = 9.6 s. This gives a factor of 5 atom production per time unit at 450 GeV/c. With this additional increase the number of produced atoms at the same intensity of the secondary particles is more than an order of magnitude higher than at 24 GeV/c.

Note also that the soft proton background at 450 GeV/c is more than an order of magnitude slower than at 24 GeV/c [31, 28], thus decreasing by an order of magnitude the background of $p\pi^-$ pairs relative to the $K^+\pi^-$ pairs.

4.3 Calculations of the correlation function $R(\vec{p_1}, \vec{p_2}, s)$ at a proton momentum of 24 and 450 GeV/c for the π^+K^-, $K^+\pi^-$ and $\pi^+\pi^-$ pairs with a small relative momentum.

The differential inclusive yield of atom production in (4) is expressed in terms of the double differential yield of two constituent particles. We obtained this yield using the FTF generator. We can also use the FTF to determine the correlation function (5) which allows the uncertainty in the minimum value ofW_A^N to be evaluated. This factor for the momentum interval of the DIRAC setup is presented in Fig.7. It shows that the factor R for $\pi^+\pi^-$ pairs at 24 GeV/c decreases from 1.25 (p_{pair} = 3 GeV/c) down to 0.5 (p_{pair} = 9 GeV/c). For $K\pi$ pairs R decreases from 1 (3 GeV/c) down to 0.5 (10 GeV/c). This decrease is partially due to conservation law constrains. The value of R at 450 GeV/c practically does not depend on the pair momentum and the polar angle.

As we can see from Fig.7, the correlation function R for all kinds of pairs is smaller at 24 GeV/c than at 450 GeV/c for all pair momenta. The calculation of the relative atom yields W_A^N with $R = 1$ gives us the minimum value of W_A^N. In this case the error of W_A^N depends only on the uncertainties of the inclusive cross section description by the FTF. These uncertainties can be evaluated from the experimental data analysis.

4.4 The dependence of the atom and charged particle production on the target material.

There was studied the dependence of charged particle and atom yields on the target material. Three materials were used: Be, Ni and Pt. These yields for the case of charged particles are shown on Fig.8 as dependence on particle momentum at 450 GeV/c and $\theta_{lab} = 4°$. One can see that the flux of charged particles increases 1.8 times with growth

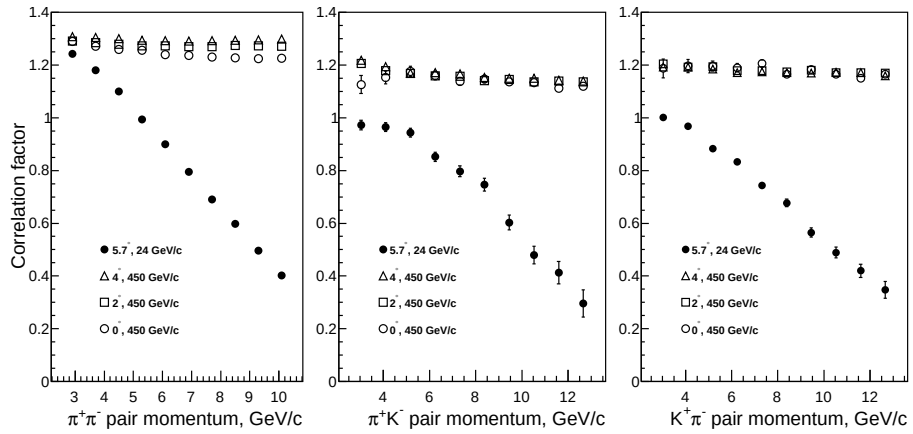

Figure 7: The dependence of correlation factor R for the $\pi^+\pi^-$, π^+K^- and $K^+\pi^-$ pairs in the DIRAC setup on their momentum in l.s. at 450 GeV/c and emission angles $\theta_{lab} = 0°$, 2°, 4° and at 24 GeV/c and the emission angle $\theta_{lab} = 5.7°$.

of nucleus atomic number from Be to Pt.

The productions of atoms integrated over the setup momentum intervals at different target materials at 450 GeV/c and $\theta_{lab} = 4°$ are shown in Tab.3. One can see that the ratio of atom productions between Ni and Be is about 3 which is about the square of charged particle intensity ratio in accordance with the atom inclusive cross section (2).

Table 3: The yields ($dN/dp[(GeV/c \times msr)^{-1}] \times 10^9$) of the $\pi^+\pi^-$, π^+K^- and $K^+\pi^-$ atoms at 450 GeV/c and an emission angle $\theta_{lab} = 4°$ for the Be, Ni and Pt targets.

Atoms	Target		
	Be	Ni	Pt
$A_{2\pi}$	1.3×10^{-8}	1.9×10^{-8}	3.6×10^{-8}
$A_{K^-\pi^+}$	3.4×10^{-10}	8.8×10^{-10}	10.2×10^{-10}
$A_{K^+\pi^-}$	5.2×10^{-10}	9.7×10^{-10}	16.7×10^{-10}

5 On the accuracy of the FTF simulation results.

As was shown in section 4.3 the error of $W_A^N(R = 1)$ depends only on the uncertainty in FTF description of the single particle yield, which we can obtain from the experimental distributions (Figs.1-3).

For $A_{2\pi}$ at 24 GeV/c we compared the MC and experimental products (PROD) of the π^+ and π^- distributions (Fig.1) in the pion momentum interval of 1-3 GeV/c and for the polar angle of 60-100 mrad. The ratio of the products is $K_{24\pi^+\pi^-} = PROD^{exp}_{24\pi^+\pi^-}/PROD^{MC}_{24\pi^+\pi^-}$ = 1.16±0.06.

For $A_{K^+\pi^-}$ at 24 GeV/c we compared the MC and experimental products of the K^+ (Fig.2, 20-140 mrad) and π^- distributions (Fig.1, 60-100 mrad) in the kaon momentum in-

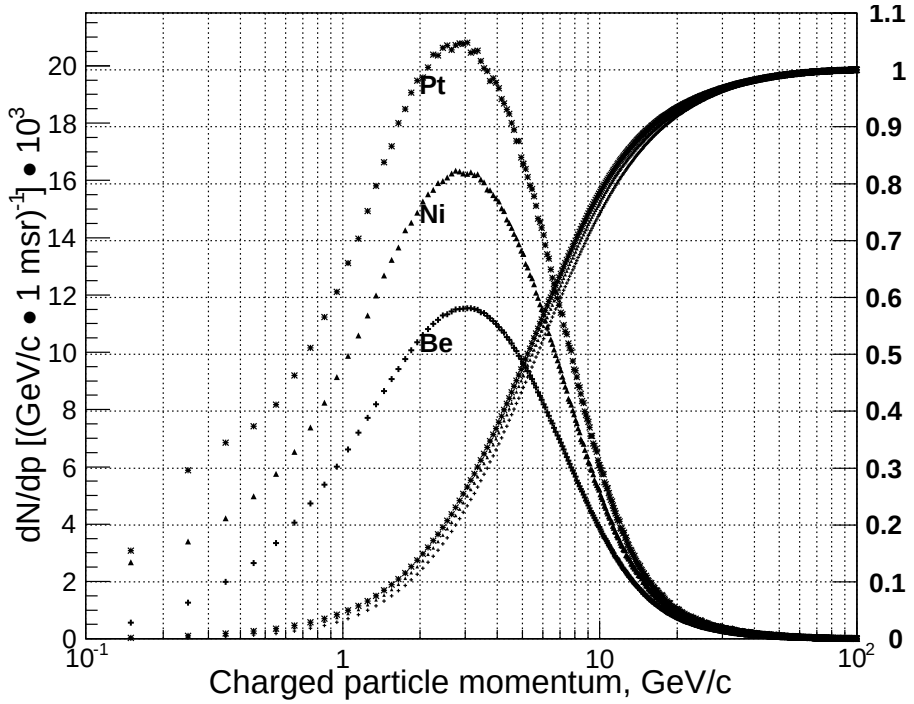

Figure 8: The total yield of the charged particles ($\pi^{\pm}$, $K^{\pm}$, p and $\bar{p}$) per p-nucleus (Be, Ni and Pt) interaction event at 450 GeV/c and an emission angles $\theta_{lab} = 4^{\circ}$ as a function of their momentum in l.s. for the solid angle of 10^{-3} sr. The integrated and normalized-to-unity distributions are also shown.

terval of 4-7 GeV/c. The ratio of the products is $K_{24K^+\pi^-} = PROD^{exp}_{24K^+\pi^-}/PROD^{MC}_{24K^+\pi^-}$ = 0.78±0.06.

For $A_{K^-\pi^+}$ at 24 GeV/c we compared the MC and experimental products of the K^- (Fig.2, 100-140 mrad) and π^+ distributions (Fig.1, 60-100 mrad) in the kaon momentum interval of 4-7 GeV/c. The ratio of products is $K_{24K^-\pi^+} = PROD^{exp}_{24K^-\pi^+}/PROD^{MC}_{24K^-\pi^+}$ = 0.90±0.07.

At 450 GeV/c we used the point in the experimental invariant inclusive cross sections of π^+, π^-, K^+ and K^- at $p_{\pi^+,\pi^-,K^+,K^-} = 7$ GeV/c. The same ratios at 450 GeV/c ($K_{450\pi^+\pi^-}$,$K_{450K^+\pi^-}$ and $K_{450K^-\pi^+}$) are 0.87±0.13, 0.75±0.12 and 0.82±0.17 respectively. We used these correction factors to estimate the minimal gain of the atom production at 450 GeV/c in comparison with that at 24 GeV/c (Tables 4,5).

The $W_A(R = 1)$ and $W^N_A(R = 1)$ values are presented in Table 4. The minimal ratios of $A_{2\pi}$, $A_{\pi^+K^-}$ and $A_{\pi^-K^+}$ at 450 GeV/c and 24 GeV/c are 9.7±1.5, 45±8 and 18.6±4.1 respectively. Thus, even the minimal yields of $A_{\pi^+K^-}$ and $A_{\pi^-K^+}$ at 450 GeV/c are more than by an order of magnitude larger that the yields at 24 GeV/c.

Table 4: The yield $W_A(R=1)$ of $\pi^+\pi^-$, π^+K^- and $K^+\pi^-$ atoms with $R=1$ into the aperture of 10^{-3} sr with allowance for the setup acceptance and pion and kaon decays per pNi interaction event at 24 and 450 GeV/c versus the emission angle θ_{lab}. The ratio $W_A^N(R=1) = W_A(R=1,\ 450\ GeV/c)/W_A(R=1,\ 5.7^\circ, 24\ GeV/c)$ gives the minimum ratio of the atom yields at 450 GeV/c and 24 GeV/c.

θ_{lab}	5.7°	4°	2°	0°
E_p	24 GeV/c	450 GeV/c	450 GeV/c	450 GeV
Yield of $\pi^+\pi^-$ atoms				
$W_A(R=1)\times 10^9$	1.73±0.09	17±2	30±5	39±6
$W_A^N(R=1)$	1	9.7±1.5	17.5±2.8	22.7±3.6
Yield of π^+K^- atoms				
$W_A(R=1)\times 10^9$	0.015±0.001	0.66±0.11	1.31±0.21	1.52±0.24
$(W_A^N(R=1))$	1	45±8	87±15	104±18
Yield of $K^+\pi^-$ atoms				
$W_A(R=1)\times 10^9$	0.042±0.003	0.79±0.16	1.8±0.4	2.2±0.5
$W_A^N(R=1)$	1	18.6±4.1	41±9	52±11

6 The prospects of the long-lived dimesoatom investigation at 450 GeV/c and the long-lived dimesoatom beam creation.

As mentioned in the introduction the secondary particle flux intensity restricted the primary proton beam intensity in the experiment on the observation of long-lived $A_{2\pi}$ at a level of 3×10^{11} protons/spill (time of spill = 0.45 s) and thus the number of atoms produced within a time unit. The long-lived atom production within a time unit can be increased significantly if by installing a collimator behind the Be target and applying the vertical magnetic field behind it, which deflects soft particles with a momentum below 10 GeV/c from the setup aperture. In this case the total flux of the secondary charged particles into the setup aperture at an angle of 4° can be decreased by a factor of 5 (Fig.4) and hence the intensity of the primary proton beam and the number of produced atoms can be increased by the same factor. In this scheme the number of generated long-lived atoms at 450 GeV/c and $\theta_{lab} = 4^\circ$ per unit time can be obtained by multiplying the table 2 values, the beam time increasing (factor 5) and the beam intensity enlarge. It gives the increasing 370, 1600 and 750 times for long-lived $A_{2\pi}$, $A_{\pi^+K^-}$ and $A_{\pi^-K^+}$ atom production.

If the Be target is replaced by a target with larger atomic number, the probability of long-lived atom production will increase as the probability of atom production per p-nucleus interaction and the probability of atom excitation in the target in the long-lived state will grow both.

In the DIRAC experiment $n_{AL} = 436\pm 57\text{stat}\pm 23\text{syst}$ atomic pairs from the long-lived atom breakup in the Pt foil were detected. The main contribution to the statistical error came from the background of the $\pi^+\pi^-$ pairs generated in the Be target. This background

Table 5: The relative yields $W_A(R=1)/W_{ch}$ of the $\pi^+\pi^-$, π^+K^-, and $K^+\pi^-$ atoms into the aperture of 10^{-3} sr with allowance for the setup acceptance and pion and kaon decays per pNi interaction event at 24 and 450 GeV/c versus the emission angle θ_{lab}. $(W_A(R=1)/W_{ch})^N$=$(W_A(R=1)/W_{ch})/((W_A(R=1)/W_{ch})(5.7^\circ, 24\ GeV/c))$.

θ_{lab}	5.7°	4°	2°	0°
E_p	24 GeV/c	450 GeV/c	450 GeV/c	450 GeV
Yield of $\pi^+\pi^-$ atoms				
$W_A(R=1)/W_{ch}\times 10^9$	78±4	121±14	60±10	13.4±2.1
$(W_A(R=1)/W_{ch})^N$	1	1.55±0.20	0.77±0.13	0.17±0.03
Yield of π^+K^- atoms				
$W_A(R=1)/W_{ch}\times 10^9$	0.66±0.04	4.7±0.8	2.6±0.4	0.52±0.08
$(W_A(R=1)/W_{ch})^N$	1	7.±1.	3.9±0.7	0.79 ±0.13
Yield of $K^+\pi^-$ atoms				
$W_A(R=1)/W_{ch}\times 10^9$	1.91±0.14	5.6±1.1	3.6±0.8	0.76±0.17
$(W_A(R=1)/W_{ch})^N$	1	2.9±0.6	1.9±0.4	0.40±0.09

is 40 times higher than the signal n_{AL}. After the magnetic field is applied, the charged particles with the momentum lower than 10 GeV/c will not be detected by the setup detectors behind the spectrometer magnet and the background will be decreased very significantly. In the experiments [33] on the $\pi\mu$ atom observation and investigation at the conditions similar to the above scheme with the magnetic field the background was indeed a few percent relative to the $\pi\mu$ pairs from the atom breakup in the thin foil.

Therefore, with the applied magnetic field, the error of n_{AL} will be significantly smaller than in the DIRAC experiment as a result of not only increase in the atomic pair statistic by more than two orders of magnitude but also as result of the background suppression by more than two orders of magnitude. Then the main source of the systematic error in n_{AL} will be uncertainty in the thickness of the Pt foil which can be significantly decreased.

In the experiment where some part of the charged particles is deflected from the setup aperture by the additional magnetic field , the number of the detected $\pi^+\pi^-$ atomic pairs per time unit will increase less than the number of the produced long-lived atoms. In this scheme the distance between the Be target and the Pt foil must be larger than in the DIRAC experiment (96 mm) and part of the long-lived atoms will decay reaching the foil. The decay probability for the part of the atoms with the orbital momentum projection in the magnetic field direction $m=0$ also increases. Nevertheless the number of detected atomic pairs per time unit will be larger by two orders of magnitude than in the DIRAC experiment. The large statistics of the atomic pairs and the low level of the background will open up a possibility of using the resonance method [16] for measuring the $A_{2\pi}$ Lamb shift.

In this method the long-lived atoms cross an electric or magnetic field which is a periodic function of the coordinate along the beam axis with the frequency ω_L. In the atom c.m.s. this field is transformed into an electric field oscillating in time with the frequency $\tilde{\omega}=\omega_L\gamma$, where γ is the atom Lorentz factor. For a set of γ the value of $\tilde{\omega}$ coincides with the atom's intrinsic frequencies $\Omega_n=(E_{np}-E_{ns})/\hbar$, where E_{ns} and E_{np}

are the atomic level energies and $\hbar$ is the Planck constant. In this case the atoms with the Lorentz factors from the equation

$$\gamma_n \omega_L = \Omega_n \tag{6}$$

oscillate between $np-ns$ states. The short-lived ns-state atoms decay completely and the number of dimesoatoms behind the resonator with Lorentz factors around γ_n is decreased.

Behind the resonator a thin Pt foil will be installed in which more than 90% of long-lived atoms break up. In the momentum spectrum of atomic pairs there will also be the set of minima. Measuring the positions of the γ_n minima and knowing the resonator frequency, ω_L we can evaluate from equation (6) the energy splitting between $np-ns$ states. The part of the energy splitting connected with the vacuum polarization and other electromagnetic effects are about 20% of the total energy splitting. Subtraction of this part will yield the strong part of the energy splitting depending on the $\pi\pi$ scattering length combination $2a_0 + a_2$. The difference of this method from other methods([17] and [7]) for $\pi\pi$ scattering length evaluation is that the measurement of the total energy splitting uses only the Lorentz transformation and quantum mechanics in the experimental data analysis.

A large yield of $A_{\pi^+K^-}$ and $A_{\pi^-K^+}$ will allow simultaneous measurement of these atoms and of the $A_{2\pi}$ Lamb shift using the symmetrical setup geometry which is optimal only for the $\pi^+\pi^-$ atomic pair detection. The $A_{\pi^+K^-}$ and $A_{\pi^-K^+}$ energy splitting can be measured in the asymmetric geometry of the setup with allowance for the fact that in πK atomic pairs the K meson momentum is 3.6 times higher than the pion momentum.

In the DIRAC experiments thin targets were used with the nuclear efficiency 2.5×10^{-4} for the long-lived atoms and 6.5×10^{-4} for the short-lived atoms. Therefore the disturbance of the proton beam is insignificant and this experiment can be performed simultaneously with the other experiments.

7 Conclusion

The performed analysis has shown that the dimesoatom production in the p-nucleus interaction can be increased by more than an order of magnitude if the incident proton momentum is changed from 24 GeV/c to 450 GeV/c. The yield of $A_{2\pi}$ ($A_{\pi^+K^-}$, $A_{\pi^-K^+}$) in the momentum interval of the DIRAC experiment 2.5-10.5 GeV/c (5-14 GeV/c) at 450 GeV/c and $\theta_{lab} = 4^\circ$ is 17 (38, 16) times higher than their production at 24 GeV/c and $\theta_{lab} = 5.7^\circ$ (Table 1). The yields are twice as high for $\theta_{lab} = 2^\circ$. All these values were calculated by integration of the dedicated atomic momentum spectrum in the intervals mentioned above. If one takes into account the DIRAC setup acceptance (Table 2), the relative yields of $A_{2\pi}$, $A_{\pi^+K^-}$ and $A_{\pi^-K^+}$ at $\theta_{lab} = 4^\circ$ (2°) at 450 GeV/c are 15(28), 67(131) and 31(68) times higher than at 24 GeV/c. The minimum values of these ratios were evaluated in the model-independent way and the following results (Table 4) were obtained at $\theta_{lab} = 4^\circ(2^\circ)$: 9.7±1.5 (17.5±2.8), 45±8 (87±15) and 18.6±4.1 (41±9). They confirm that even the minimum yields at 450 GeV/c are higher by more than an order of magnitude than at 24 GeV/c.

In the experiments on the lifetime measurement of short-lived $A_{2\pi}$, $A_{\pi^+K^-}$ and $A_{\pi^-K^+}$ the secondary particle flux intensity in the DIRAC experiment restricted the primary proton beam intensity and the number of detected atoms within a time unit. For the

same total flux intensity of the charged particles as in the DIRAC experiment the yields of $A_{2\pi}$, $A_{\pi^+K^-}$ and $A_{\pi^-K^+}$ at 450 GeV/c and $\theta_{lab} = 4^\circ$ are 2.7, 5.8 and 2.5 times higher respectively. As mentioned in section 4.2, the beam time per supersycle on the SPS is 5 times higher than on the PS. Therefore the number of $A_{2\pi}$, $A_{\pi^+K^-}$, and $A_{\pi^-K^+}$ per time unit can be 14, 29 and 12 times higher respectively.

In the DIRAC experiment, 436±57stat±23syst $\pi^+\pi^-$ atomic pairs from the breakup of long-lived atoms in the Pt foil were detected in pBe interactions at 2/3 of the existing statistics. The main contribution to the statistical error comes from the background of $\pi^+\pi^-$ pairs generated in the Be target which is 40 times higher than the number of atomic pairs. It was discussed in section 6 that the magnet installation behind the Be target allows the proton beam intensity to be increased by an order of magnitude and the background to be decreased by about two orders of magnitude. The statistical error significantly decreases, and the systematic error can also be suppressed. In this scheme the number of produced $\pi^+\pi^-$, π^+K^-, and $K^+\pi^-$ atoms per time unit increases by a factor of 370, 1600 and 750 respectively. The number of $\pi^+\pi^-$ atomic pairs per time unit increases less than the number of atoms. Nevertheless, this increase is still two orders of magnitude. The large statistics and significant background suppression will allow using the model independent analysis for measurements of the Lamb shift and combination of $\pi\pi$ scattering lengths $2a_0 + a_2$. This analysis involves only the Lorentz transformation and quantum mechanics.

8 Acknowledgments

We are grateful to M.Gadzitski and A.Korzenev for providing us with the unpublished data on inclusive cross sections for pC interactions at 31 GeV/c. We are also grateful to V.Uzhinsky for the discussion on the FTF generator and to P.Shcliapnikov for helpful comments.

References

[1] J.Uretsky and J.Palfrey, Phys. Rev. **121** (1961) 1798.

[2] S.M.Bilenky et al., Yad. Phys. **10** (1969) 812; (Sov. J. Nucl. Phys. **10** (1969) 469).

[3] J. Gasser et al., Phys. Rev. **D64** (2001) 016008; he*p*-ph/0103157.

[4] J.Schweizer, Phys. Lett. **B587** (2004) 33; J. Schweizer, Eur.Phys.J. C 36 (2004) 483, arXiv:hep-ph/0405034.

[5] A.Adeva et al., J. Phys. G: Nucl. Part. Phys. **30** (2004) 1929.

[6] B.Adeva at al., Phys. Lett. **B619** (2005) 50.

[7] A.Adeva et al., Phys. Lett. **B704** (2011) 24.

[8] A.Adeva et al., Phys. Lett. **B735** (2014) 288.

[9] A.Adeva et al., Phys. Lett., **B751** (2015) 12., arXiv:1508.04712;

[10] P.Buttker, S.Descotes-Genon, B.Moussallam, Eur. Phys. J. **c33** (2004) 409. J. High Energy Phys. **O405**(2004) 036 he*p*-ph/0404150.

[11] V.Bernard et al., Nucl. Phys. **B357** (1991) 129., Phys. Rev. **D43** (1991) 3557.

[12] J.Bijnens et al., J. High Energy Phys. **O405**(2004) 036 hep-ph/0404150.

[13] C.B.Lang, et al., Phys. Rev. **D86** (2012) 054508.

[14] L.Nemenov, Yad. Fiz. **41** (1985) 980.

[15] L.L.Nemenov and V.D.Ovsiannikov, Phys. Lett. **B514** (2001) 247.

[16] L.L.Nemenov, V.D.Ovsyannikov, E.V.Chaplygin, Nucl. Phys. **A710** (2002) 303.

[17] J.R.Bateley at al., Eur. Phys. J. **C64** (2009) 589.

[18] J.R.Bateley at al., Eur. Phys. J. **C70** (2010) 635.

[19] A.Adeva et al., CERN Preprint,CERN-PH-EP-2015-147, 2015;

[20] O.E.Gorchakov et al., Yad. Fiz. **59** (1996) 2015;(Phys. At. Nucl. **59** (1996) 1942).

[21] O.E.Gorchakov et al., Yad. Fiz. **63** (2000) 1936;(Phys. At. Nucl. **63** (2000) 1847).

[22] O.Gorchakov and L.Nemenov[JINR], DIRAC Note **2012-6**.

[23] Sjöstrand T., Bengtsson M., Com. Phys. Comm. **43** (1987) 367.

[24] V.Uzhinsky, arXiv:1109.6768[hep-ph], 2011.

[25] S. Agostinelli et al., NIMPA **506** (2003) 250.

[26] O.Gorchakov and L.Nemenov[JINR], DIRAC Note **2015-3**.

[27] N.Abgrall at al , Phys.Rev C84 034604(2011), Phys.Rev. **C85** 035210(2012), Private communication.

[28] G.Ambrosini at al.,Eur.Phys.J. **C10** (1999) 605.

[29] D.S.Barton at al.,Phys. Rev. **D27** (1983) 2580.

[30] Grishin V.G., Inclusive processes in hadron interactions at high energy. Energoizdat, Moscow 1982, p. 131 (in Russian).

[31] Eichten T. et al., Nucl. Phys. **B44** (1972) 333.

[32] A.Adeva et al., CERN Preprint, CERN-PH-EP-2015-175, 3315.

[33] S.H. Aronson et al., Phys.Rev.Lett. 48 (1982) 1078-1081.

[34] G.V.Efimov at al.,Yad.Fiz.44(1986),460;(Sov.J.Nucl.Phys. 44 (1986) 296.

[35] A.Karimhodjaev and R.N.Faustov,Yad.Fiz.29 (1979) 463;Sov.J.NuclPhys. 29 (1979) 232.